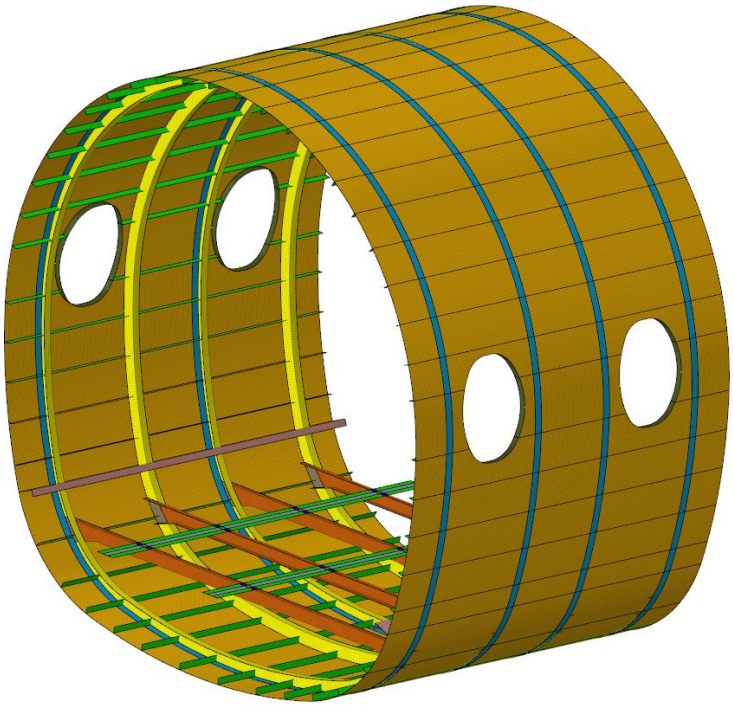

The effect of fuselage cross-sectional shape on strength and drag for a short-haul aircraft

A case study for a short range commercial aircraft

Master's thesis in Applied Mechanics

SENA OTLU

DEPARTMENT OF INDUSTRIAL AND MATERIALS SCIENCE

CHALMERS UNIVERSITY OF TECHNOLOGY
Gothenburg, Sweden 2023
www.chalmers.se

Master's thesis 2023

The effect of fuselage cross-sectional shape on strength and drag for a short-haul aircraft

A case study for a short range commercial aircraft

SENA OTLU

CHALMERS
UNIVERSITY OF TECHNOLOGY

Department of Industrial and Materials Science
Division of Material and Computational Mechanics
Chalmers University of Technology
Gothenburg, Sweden 2023

The effect of fuselage cross-sectional shape on strength and drag for a short-haul aircraft
A case study for a short range commercial aircraft
SENA OTLU

Thesis partner: Rushabh Ashok Kathote, Linköping University
Academic Supervisor and Examiner: Martin Fagerström, Division of Material and Computational Mechanics, Department of Industrial and Materials Science
Industrial Supervisor: William Tempel De Donato, Leandro G Maia, Heart Aerospace
The effect of fuselage cross-sectional shape on strength and drag for a short-haul aircraft 2023
Department of Industrial and Materials Science
Division of Material and Computational Mechanics
Chalmers University of Technology
SE-412 96 Gothenburg
Telephone +46 31 772 1000

Cover: The center fuselage of the aircraft meshed in HYPERMESH.

Typeset in LaTeX
Printed by Chalmers Reproservice
Gothenburg, Sweden 2023

Study the effect of fuselage cross-section on strength and drag
for a short range commercial aircraft
SENA OTLU
Department of Some Subject or Technology
Chalmers University of Technology

Abstract

Aviation, which has a history of more than two thousand years, starts with a simple kite. Now in the 21st century, aircraft containing millions of parts are being developed causing a lot of emissions which have the main contributor as the fuel consumption. The aerospace industry goes out to find different solutions to reduce emissions of greenhouse gases from aircraft, which has led to the implementation of new power sources like electricity, liquid hydrogen, and sustainable aviation fuel (SAF). Using electric motors has also a cost advantage which reduces maintenance costs by 90 percent compared to turboprops, and most importantly, the cost of the energy of the engines goes down by 50-75 percent [1].

In this master thesis, the efficiency study of the airframes of 2+1 seat configuration for the short-haul commercial airliner was performed by finite element methods under the specified pressure force. The displacement, stress, weight, and drag results of four main cross-sections of the center fuselage were compared to identify the most effective cross-section.

Keywords: finite element method, aircraft, cross-section, displacement, stress, drag

Acknowledgements

This master thesis was performed at Heart Aerospace, Gothenburg, Sweden during the spring semester of 2022.

I would like to give special thanks to my thesis partner Rushabh Kathote who worked with me on this project for brainstorming, discussions, and being a teammate during all the steps.

I would like to warmer thank my industrial supervisors William Tempel De Donato and Leandro G Maia for their support and guidance all along. I would like to thank my academic supervisor and examiner Martin Fagerström, Material and Computational Mechanics to provide feedback, motivating, and supporting me during the thesis.

Besides my thesis partner and supervisors, I would like to thank my mother Yildiz Özaslan, and my siblings Esra Otlu and Baran Otlu who have been supporting my career goals all my life.

Additionally, I appreciate and thank you for having a scholarship from the Republic of Turkiye the Ministry of National Education during my master's education.

Sena Otlu, Gothenburg, June 2022

List of Acronyms

Below is the list of acronyms that have been used throughout this thesis listed in alphabetical order:

AC	Aircraft
CAD	Computer-Aided Design
CV1	Circular Cross Section Version 1
CV2	Circular Cross Section Version 2
C1DBV1	Comfort1 Double-Bubble Cross Section Version 1
C1DBV2	Comfort1 Double-Bubble Cross Section Version 2
C2DBV1	Comfort2 Double-Bubble Cross Section Version 1
C2DBV2	Comfort2 Double-Bubble Cross Section Version 2
C2DBV3	Comfort2 Double-Bubble Cross Section Version 3
DBV1	Double-Bubble Cross Section Version 1
DBV2	Double-Bubble Cross Section Version 2
EASA	The European Aviation Safety Agency
EASA CS-23	The European Aviation Safety Agency Certification Specification 23
EU	European Union
FBV1	Flat Bottom Cross Section Version 1
FBV2	Flat Bottom Cross Section Version 2
FEM	Finite Element Methods
FOS	Factor of Safety
MPC	Multi Point Constraint
RBE2	Rigid Body Element (Kinematic Coupling)
RBE3	Rigid Body Element (Distributed Coupling)
SAF	Sustainable Aviation Fuel
SPC	Single Point Constraint

Contents

List of Figures

List of Tables

1
Introduction

1.1 Background

One of the main issues with using electric power is storing the batteries in the aircraft structure. In contrast to jet fuel, which is liquid and therefore can be stored in the spaces between the structures in the wing or the fuselage. The battery packs are modular and associated with higher safety requirements. This means that they cannot be stored everywhere in the aircraft. This must be considered already during the conceptual design phase, where choosing the right cross-section plays a crucial role in the overall performance and efficiency of the aircraft.

1.1.1 Short-Haul Airliner

In aviation, if the distance of flight is shorter than 1100-1500 km (600-800 nmi), the flight is called short-haul. A regional airliner is designed to fly short-haul up to 100 passengers and is regulated by the European Aviation Safety Agency (EASA) if the manufacturer, maintainer, or user is under the regulatory oversight of the European Union (EU) and the Member States [3]. The short-haul airliners have a seating capacity of 20 to 80 seats with configurations of 1+1 or 2+1 since the aircraft with more seat for each seating row in the passenger's cabin compartment (i.e. 2+2) need bigger cross-section area that means more drag and more fuel consumption. The cabin interior configuration of the 2+1 airliner, EMB-145 by Embraer [4], can be seen in Figure 1.1. In this configuration, the distance between the seats, the height of the cabin ceiling, the seat measures that allow the passenger to sit in a healthy position, and the distance between the seats are also regulated by EASA [5]. Furthermore, different cross-sections of different airliners can be seen in Figure 1.2. Gulfstream G650 has up to 15 seats [6], Bombardier Global Express has up to 19 seats [7], Gulfstream G550 has up to 19 seats [8], Antonov AN-148/AN-158 has up to 92 seats [9], and Embraer Lineage has up to 19 seats [10]. Antonov AN-148/AN-158 has the biggest cross-section and the highest number of passengers since its flight range is longer than 1500 km. Although all these four aircraft are not in the same class, short-haul airliners, their center fuselage cross-sections which is the passenger cabin were inspected to have an idea of the cabin interiors. It is more convenient to carry more passengers with bigger airliners for longer distances. Gulfstream G550 and Embraer Lineage have the same passenger capacity, but the cross-sections of the cabin, and fuselage, are different in shape and size. The differences in cross-sectional areas can be explained due to the different devices used by each aircraft, and the different wing and tail configurations.

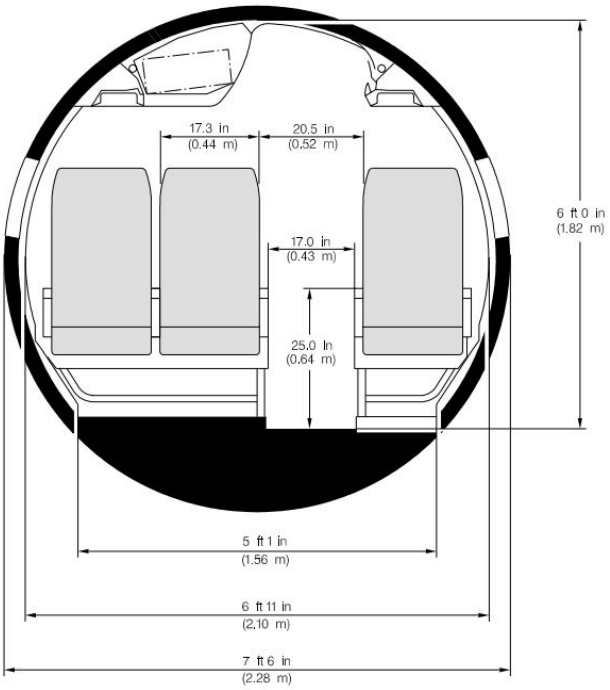

Figure 1.1: EMB-145 Passenger Cabin Cross-Section

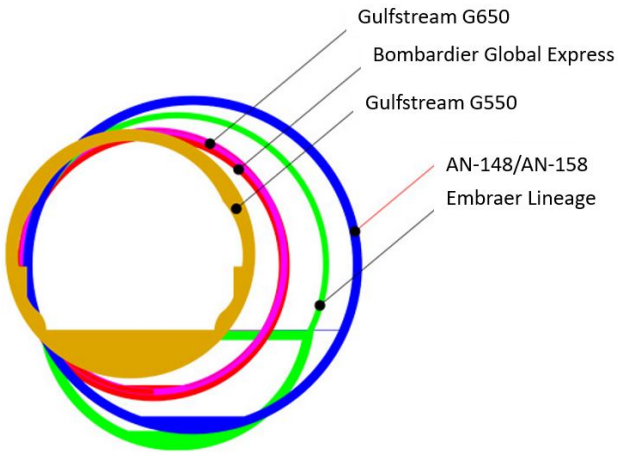

Figure 1.2: Cabin cross-section comparison of different airliners.

1.1.2 Electrical Aircraft

An aircraft powered by electricity to drive the engine is called an electrical aircraft. The most common method to supply electricity is batteries. The very first electrical aircraft was flown by brothers Albert Charles Tissandier and Gaston Tissandier in 1883 in France [11], see Figure 1.3. Today, there are more than 10 electric aircraft known to be under development, including electrical helicopters, passenger planes, private jets, and small planes.

Batteries have different requirements when compared to jet fuel, so they must be stored in the aircraft by different methods. The battery cells must be accessible in order to be taken out and charged at certain intervals. Also, due to various safety requirements, such as the requirements for spacing between battery cells and harness systems, other structural elements in the aircraft need to be designed accordingly.

Figure 1.3: Albert Tissandier (left) and Gaston Tissandier (right) in the gondola of their electrical air-balloon.

1.1.2.1 State of the Art for Electrical Aircraft

Before 2030, many companies are working to take their place in the sustainable aviation market. Some of those can be seen from Table 1.1.

Scylax Aircraft, Germany, is working with 10-seat short-haul aircraft called Scylax E10, which is aiming to be certificated in 2026 [12]. Eviation Aircraft, Israel, is developing 9-seat short-haul aircraft called The Eviation Alice, and will be certificated in 2023 [13]. One another aircraft will be certificated in 2026 is ERA (Auro Aero, France) [14] which has 19-seat.

Heart Aerospace, established in Gothenburg in 2018 is working on the design of a regional electrical aircraft for short-distance air travel which is called ES-19. The aircraft is in the conceptual phase and the flight performance, propulsion mode, and other details are being studied. This thesis is the study of fuselage cross-section effects on the strength and drag of a short-haul aircraft.

Table 1.1: Example of the companies which are developing electrical aircraft.

The Aircraft	Passenger Capacity	Presumed Certification Year	Company Name	Company Location
Es-19	19	2026	Heart Aerospace	Sweden
Scylax E10	10	2027	Scylax Aircraft	Germany
The Eviation Alice	9	2023	Eviation Aircraft	Israel
ERA	19	2026	Aura Aero	France

1.2 Aim

The purpose of the thesis is to provide data to understand the advantages and disadvantages of four different fuselage cross-sections from the points of strength and aerodynamics. At the end of the study, the deformations under the same load, the total weight of four cross-section assemblies, and their drag effects have been compared to obtain the data for the future works of Heart Aerospace.

1.3 Problem Description

An overview of a sample center fuselage cross-section is shown in Figure 1.4. The objective of the thesis was to study the effect of variation in the center fuselage cross-section on the drag and strength for a 2+1 configuration. Initially, a detailed study was to be performed on the circular fuselage design considering similar aircraft in the market. The region under the floor was not completely utilized, hence the space had to be reduced to obtain a double-bubble structure. The cross-section needed to be varied to obtain several configurations by trial and error method. With the results from all of the scenarios, sufficient data was provided describing the advantages and disadvantages of choosing a particular configuration in the aircraft. These parameters were studied in each case:

1. Passenger ergonomics
2. Strength and weight of the frame
3. Drag

1.4 Limitations

During the thesis work to be done in 20 weeks, there were some limitations due to the time period listed below.

- The study has been only done for one specific section of the fuselage: the center fuselage (passenger cabin). The front fuselage (cockpit) and the rear fuselage have not been considered.
- The fuselage with a 3 abreast configuration, which has 2 seats on one side (right/left) and 1 seat on another side (left/right) was focused on in this thesis, see Figure 1.1.

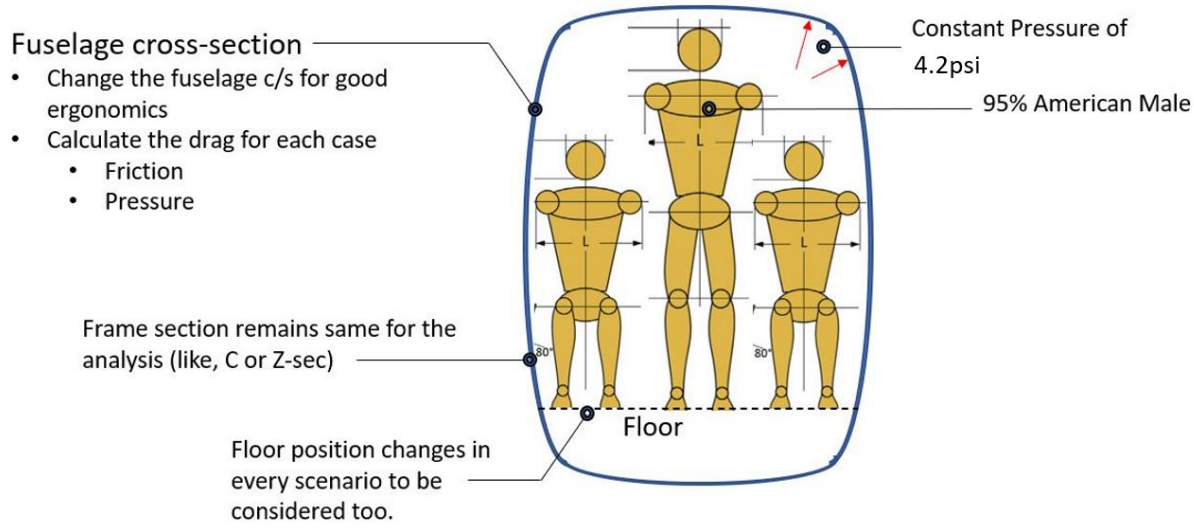

Figure 1.4: The overview of the sample of a centre fuselage cross-section.

- For the loading of the fuselage, only the pressure difference between the cabin inside and outside of the aircraft has been considered (to avoid the complexities in this study which is 4.2 psi maximum). The pressure outside the cabin, in the air, is varying between the values of 14.70 psi (at sea level, 0 C°) to 6.45 psi (at the maximum operating altitude, 20 000 ft, 0 C°) has not been taken into account.
- The center fuselage assemblies mainly consist of skin, frames, stringers, floor beams, horizontal beams, and window frames. The number of frames and windows will be the same for all four cross-section assemblies. The distances between stringers will be kept the same. All the elements of the assembly will be aluminum (Al7050-T7475) sheet metal. The material specified for the structures has not been changed during the study.
- The type of the frames has been chosen to be limited to a C-type, although the cross-section dimensions have been altered.
- Instead of computational fluid dynamics methods to calculate drag, basic equations have been used to calculate the friction drag and the pressure drag due to the limited time of the thesis study.
- Since all the inputs from other fields such as flight mechanics and, dynamics, loads, and manufacturing, the aim of the study is not taking any decision to find the best fuselage cross-section.

2

Methods

BIR YERE: inertia relief method, The problem is solved using another approach simulating the full model. The problem is solved using the inertia relied method, where the constraints are not applied on the model, but an acceleration is induced by the solver using the density values 3.2.5.2. The nastran parameter, PARAM,INREL,-2 [11], provides the solution to the problem without requiring constraints.

In this chapter, the procedures of computer-aided design (CAD) modeling, FEM analysis, and drag calculations are explained. The main aircraft configuration assumed in this thesis can be seen from Figure 2.1, which has a uniform cross-section throughout the center fuselage, an upper wing configuration, and a T-tail. After the surface models were created for each cross-section in CATIA V5 [15], the meshing process was performed with HYPERMESH [16] [17], boundary conditions were created and problem analysis steps were determined. HYPERMESH models were exported to run on NASTRAN [18] and results were observed in the models with HYPERVIEW [16] [17] after analyses were completed.

The drag estimations for each model were done by the equations and assumptions given in Section 2.3.

The weights were calculated for the assembly (model) including 4 frames, 4 floor beams, 2 rails, 4 windows, 1 horizontal beam, and almost the same number of stringers. Only the model FBV2 has extra 4 struts.

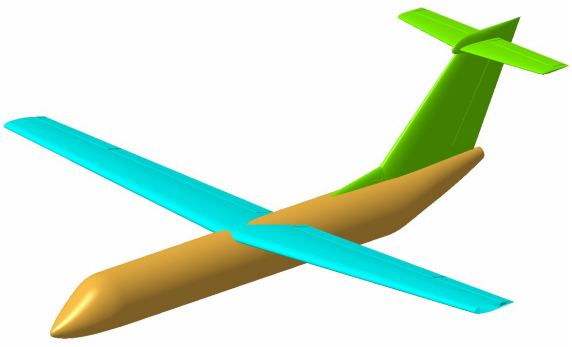

Figure 2.1: The simple aircraft model was assumed in this thesis. The golden yellow part is the fuselage, the blue part is the wing and the green part is the tail.

2.1 Design of the Fuselage Geometries in CAD

The geometry of the center fuselage, based on the initial assembly provided by engineers working in Heart Aerospace, consists of skin, frames, windows, stringers, floor beams, horizontal beams, rails, and struts. The number of stringers is slightly changing for the different cross-sections to keep the same distance between the stringers when the cross-sections are getting larger (or smaller). The main assembly of the center fuselage cross-section can be seen in Figure 2.2.

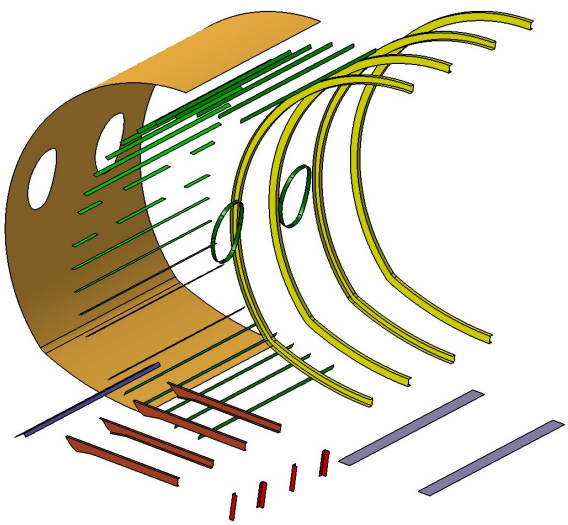

Figure 2.2: The CATIA V5 model of the cross-section which is having the flat bottom.

The requirements considered to create the cross-sections are given below.

- 95 % of approximate American male size, 175 cm, was used as the basis of the calculation of the height of the cabin and the distance between the seats of the 3 abreast 2+1 configuration.
- The same male size was used for the sitting position to calculate the curvature allowing a minimum space of the cross-section right beside the leg of the passenger.
- The seat width and length were taken from the same type of airline in the literature, which is the aircraft Embraer Regional Jet 145, see Figure 1.1.
- The approximate space required for the system installation and the devices under the floor beam level, 160 mm was provided by the engineers in the company.

The 4 main different cross-sections can be seen in Figure 2.3. First of all, the minimum circle that meets the necessary requirements was drawn in sketch mode in CATIA V5. While creating CAD model, an imaginary floor level was drawn horizontally, then the minimum distance between the uppermost and lowermost of the cross-section was specified. Then a circle was drawn and it was seen that the diameter was 2.3 meters. This corresponds to the same or similar radius as the other abreast, 2+1 airlines in the literature like Embraer Regional Jet 145.

The purpose of creating other cross-sections was to see if the possible smaller or slightly bigger cross-sections would be able to meet the requirements mentioned above. For this, a double-bubble cross-section was first modeled. The area above the floor level was kept constant at a diameter of 2.3 meters. In addition, another curve was created to define the area below the floor level where the spline option was used. The curve created with this option, spline, is the combination of more than one circle having random diameters and none of them have a diameter of 2.3 meters. As the third option, an even smaller cross-section was defined by the intersection of an upper circular segment and a lower flat edge. Finally, a fourth design was generated as a modified double-bubble cross-section modified by using circle pieces with larger diameters at the floor level instead of making it even smaller. The aim here was to examine the data that would be brought by creating a more comfortable cross-section.

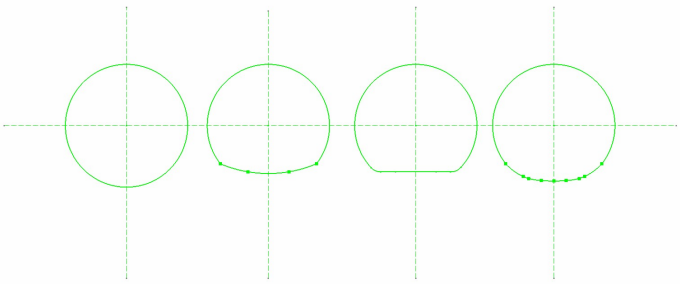

Figure 2.3: 4 main cross-sections used. Left to right: circular cross-section, double-bubble cross-section, flat bottom cross-section, and modified double-bubble cross-section (more comfortable).

After the sketches for each cross-section were completed, the skin and frame profiles were created according to these cross-sections. In the end, 11 different assemblies were achieved. To shorten the analysis time, half-scale models were also created. Together with the half-scales and the full-scales of these 11 assemblies, see Table 2.1, 17 models were analyzed. The CAD geometry properties of the detailed parts are given below.

- For each model, the skin has the same length in the x-direction, see Figure 2.4.
- The frame has C type cross-section, see Figure 2.4. The web height, the middle wall of the C shape, varies from model to model, see Table 2.1.
- The profile of the windows on the zx-plane are the same for all models, see Figure 2.5.
- The stringer has the I type cross-section and its length in the x-direction is the same as the skin length, see Figure 2.5.
- The floor beam has the C type cross-section, see Figure 2.6.
- The horizontal beam has the L type cross-section, see Figure 2.6.
- The rail for the seats has the I type cross-section, see Figure 2.7, which are located on the models asymmetrically according to the zx-plane that they have different distances to this plane because of the 2+1 configuration of the seats, see Figure 2.8.

- The strut has the L type cross-section, see Figure 2.7. Only one of the flat bottom cross-section models has this structural element, see Figure 2.2.

Table 2.1: The properties of each model were analyzed.

Cross-sections	Versions	Remarks
Circular Version 1	CV1(half) CV1(full)	50 mm frame web height
Circular Version 2	CV2(half) CV2(full)	75 mm frame web height
Double-bubble Version 1	DBV1(half) DBV1(full)	Radius change below the floor 50 mm frame web height
Double-bubble Version 2	DBV2(half) DBV2(full)	Radius change on the floor 50 mm frame web height
Flat bottom Version 1	FBV1(full)	Without struts 50 mm frame web height
Flat bottom Version 2	FBV2(half) FBV2(full)	With struts 50 mm frame web height
Comfort 1 double-bubble Version 1	C1DBV1(half) C1DBV1(full)	Curve slightly outside 50 mm frame web height
Comfort 1 double-bubble Version 1	C1DBV2(full)	Curve slightly outside 75 mm frame web height
Comfort 2 double-bubble Version 1	C2DBV1(full)	Curve more outside 50 mm frame web height
Comfort 2 double-bubble Version 2	C2DBV2(full)	Curve more outside 75 mm frame web height
Comfort 2 double-bubble Version 3	C2DBV3(full)	Curve more outside variable frame web height

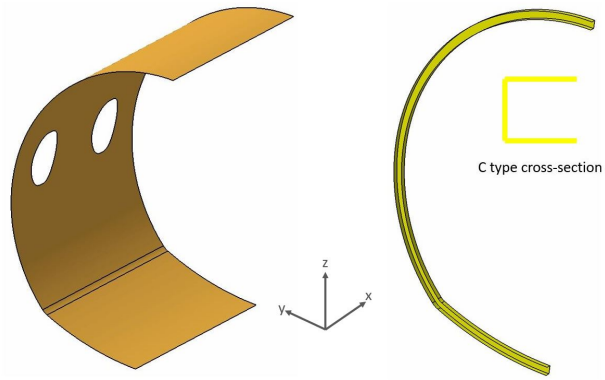

Figure 2.4: The skin with the windows holes (left) and the frame (right). The parts are representing the half of the geometries. The frame has C type cross-section.

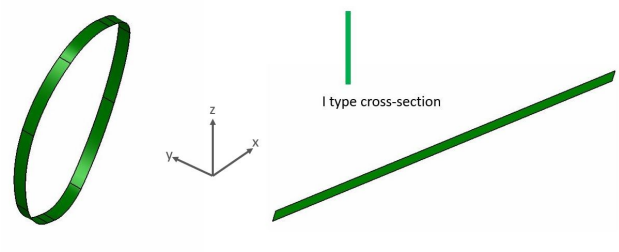

Figure 2.5: The window frame (left) and the stringer(right). The parts are representing the full geometries. The stringer has I type cross-section.

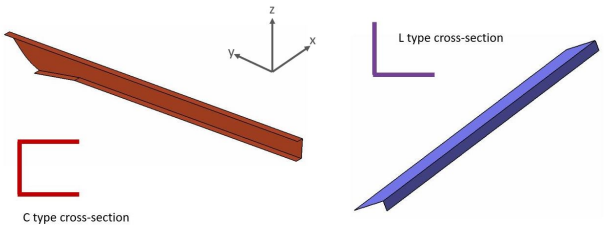

Figure 2.6: The floor beam (left) and the horizontal beam (right). The floor beam is representing the half geometry which has the C type cross-section and the horizontal beam is representing the full geometry which has the L type cross-section.

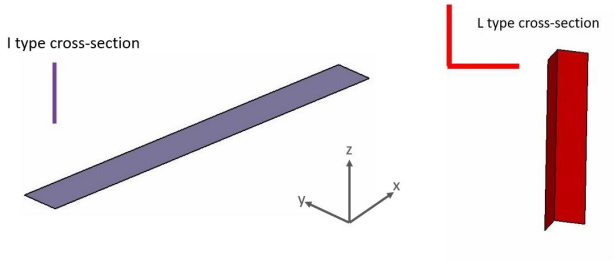

Figure 2.7: The rail (left) and the strut (right). The parts are representing the full geometries. The strut has the L type cross-section.

All 11 models have 2 windows on one side, the same length of skin in the x-direction, 4 frames, 4 floor beams, and 2 rails. Half of the main assembly without struts can be seen in Figure 2.8.

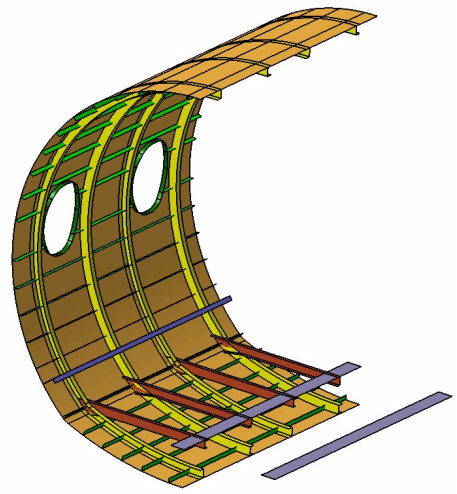

Figure 2.8: The CATIA model of DBV1. The assembly is representing the half geometry with 2 rail parts.

2.1.1 Model Specific Properties

The properties of each model are given below.

2.1.1.1 Circular Models

- Circular Version 1 (CV1): It has a 2.3 m diameter. The frames have a 50 mm web height. Both half-scale and full-scale of this model were analyzed. The half-scale model is shown in Figure 2.9.
- Circular Version 2 (CV2): It has a 2.3 m diameter. The frames have a 75 mm web height. Both half-scale and full-scale of this model were analyzed. The half-scale model is shown in Figure 2.9.

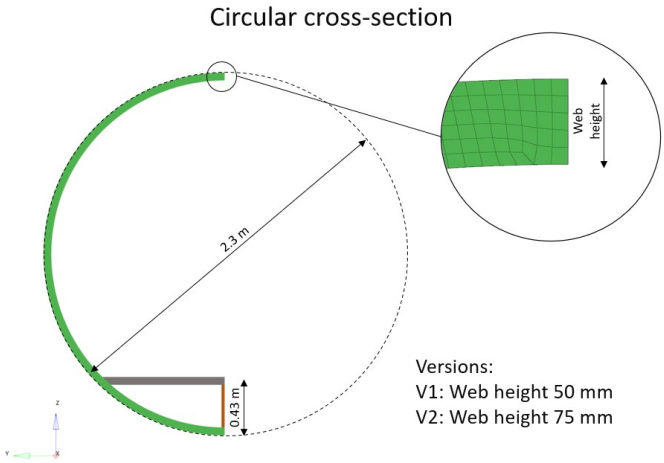

Figure 2.9: The half-scale of the circular model cross-section.

2.1.1.2 Double-Bubble Models

- Double-Bubble Version 1 (DBV1): It has a 2.3 m diameter above the transition point for the double-bubble shape. The transition point is above the floor level. The frames have a 50 mm web height. Both half-scale and full-scale of this model were analyzed. The half-scale model is shown in Figure 2.10.
- Double-Bubble Version 2 (DBV2): It has a 2.3 m diameter above the transition point for the double-bubble shape. The transition point is at the floor level. The frames have a 50 mm web height. Both half-scale and full-scale of this model were analyzed. The half-scale model is shown in Figure 2.10.

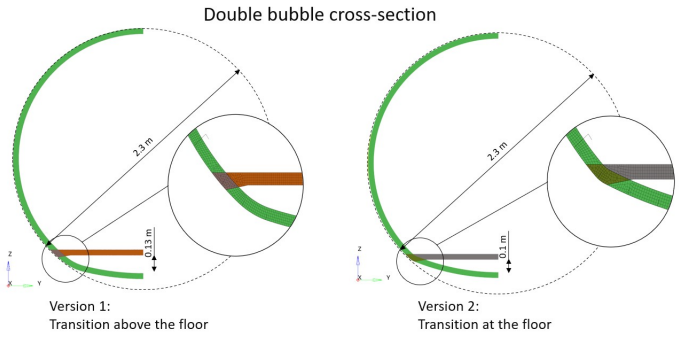

Figure 2.10: The half-scale of the double-bubble cross-section. Version 1 shows the transition point located above the floor. Version 2 shows the transition point located on the floor.

2.1.1.3 Flat Bottom Models

- Flat Bottom Version 1 (FBV1): It has a 2.3 m diameter until the flat part of the geometry. There are no struts to support the floor beams. The frames have a 50 mm web height. Only the full scale of this model was analyzed. The half-scale model is shown in Figure 2.11.
- Flat Bottom Version 2 (FBV2): It has a 2.3 m diameter until the flat part of the geometry. There are struts to support the floor beams. The frames have a

50 mm web height. Both half-scale and full-scale of this model were analyzed. The half-scale model is shown in Figure 2.11.

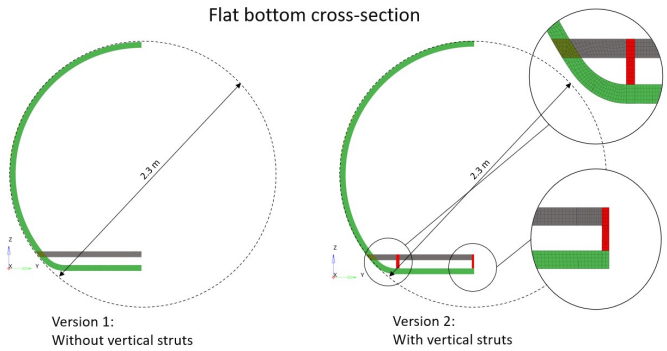

Figure 2.11: The half-scale model of the flat bottom cross-section. Version 1 shows the model without struts. Version 2 shows the model with struts.

2.1.1.4 Comfort Double-Bubble Models

- Comfort 1 Double-Bubble Version 1 (C1DBV1): It has a 2.3 m diameter above the transition point for the double-bubble shape. The curve at the floor level is slightly outside of the 2.3 diameter circle profile. The frames have a 50 mm web height. Both half-scale and full-scale of this model were analyzed. The half-scale model is shown Figure 2.12.
- Comfort 1 Double-Bubble Version 2 (C1DBV2): It has a 2.3 m diameter above the transition point for the double-bubble shape. The curve at the floor level is slightly outside of the 2.3 diameter circle profile. The frames have a 75 mm web height. Only the full-scale of this model was analyzed.
- Comfort 2 Double-Bubble Version 1 (C2DBV1): It has a 2.3 m diameter above the transition point for the double-bubble shape. The curve at the floor level is more outside of the 2.3 diameter circle profile. The frames have a 50 mm web height. Only the full-scale of this model was analyzed.
- Comfort 2 Double-Bubble Version 2 (C2DBV2): It has a 2.3 m diameter above the transition point for the double-bubble shape. The curve at the floor level is more outside of the 2.3 diameter circle profile. The frames have a 75 mm web height. Only the full scale of this model was analyzed.
- Comfort 2 Double-Bubble Version 3 (C2DBV3): It has a 2.3 m diameter above the transition point for the double-bubble shape. The curve at the floor level is more outside of the 2.3 diameter circle profile. The frames have 50 mm web height above the floor and 75 mm web height below the floor. Only the full scale of this model was analyzed.

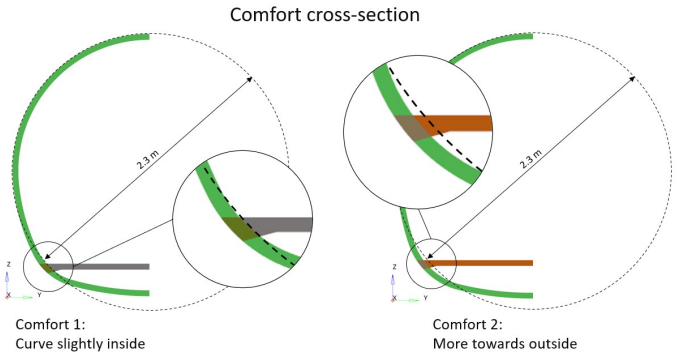

Figure 2.12: The half-scale model of the comfort double-bubble cross-section. Comfort 1 shows the slight change in the curve at the floor (curve transformation point). Comfort 2 shows more change in the curve at the floor (curve transformation point).

2.2 Meshing

The CAD surface models of each assembly were imported in HYPERMESH to mesh and define boundary conditions, material data, and individual thicknesses. The steps that were followed in HYPERMESH are given below.

- The geometry was cleaned up [1]. The common edges of the surfaces were toggled with tolerances [2]. Frames, stringers, window frames, horizontal beams, and floor beams were toggled to the skin. Stringers that have contact with the window frames were toggled to the window frames. In Figure 2.13, the yellow line means the toggled edges, the green line means 2 different surfaces sharing the same edge and the red line means fixed edges [3].

[1]The geometry cleanup in HYPERMESH is a process to prepare the surfaces of the CAD geometry to be proper to have meshed.

[2]Toggling the surfaces in HYPERMESH is a process to merge the surfaces of the CAD model to reach the consistency of the mesh of the different surfaces.

[3]The fixed edge in HYPERMESH means an edge is not shared by 2 or more different surfaces.

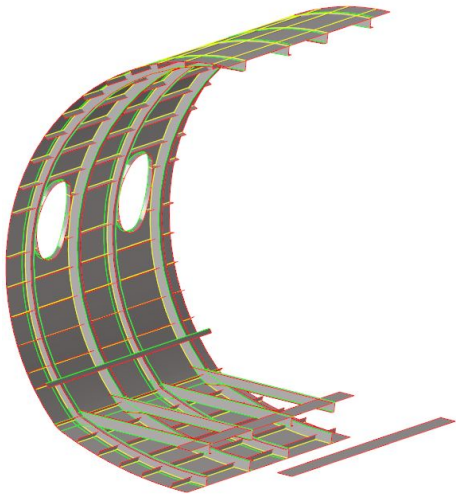

Figure 2.13: The cleaned-up model of the half-scale of the double-bubble (DBV1). Yellow lines show the toggled edges. Green lines show the shared edges by 2 different surfaces. Red lines show the fixed edges.

- The whole assembly was meshed part by part starting from the small parts to the bigger parts e.g. floor beams to skin. 10 mm x 10 mm quad element was chosen for the mesh.
- Overlapping surfaces on the geometry means overlapping meshes which are having disconnected nodes. Any overlapping meshes were split from the geometries and were treated as different surfaces. For example, frames are overlapping with the skin. Those parts of frames were split from the skin and meshed separately, see Figure 2.14. In Figure 2.15, the blue meshes belong to both the skin surface and the frames' outer flange surface. In the end, the total thickness of the skin surface and the frames' outer flange were assigned to these common blue meshes. The same procedure was done for the overlapped meshes between the floor beams and the frame web which are the brown meshes in Figure 2.15 and the overlapped meshes between the rails and the floor beams which are the dark blue and the purple meshes.

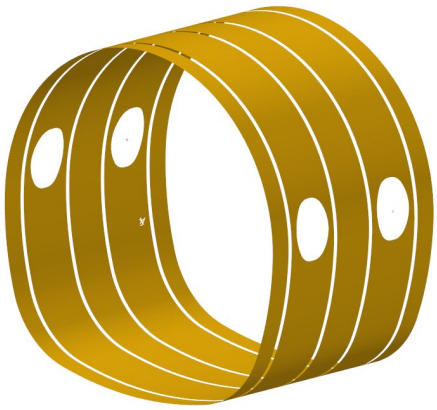

Figure 2.14: The meshed skin without the overlapping meshes.

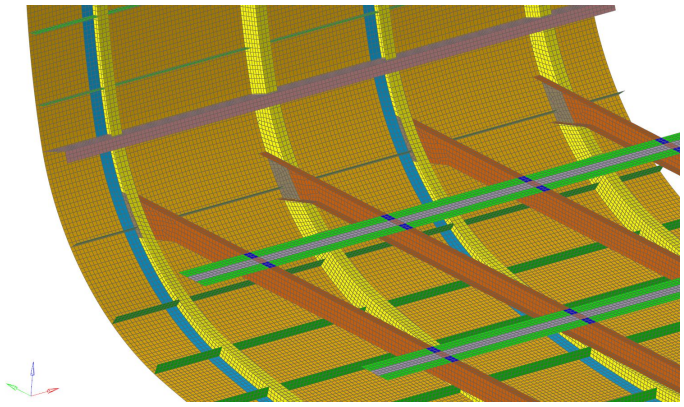

Figure 2.15: Different colors are representing the different mesh groups.

- The quality of the mesh was checked. In Figure 2.16, the failed mesh which was a very sharp corner or a corner having a very wide-angle, red-colored, and the one that had lower qualities, yellow-colored, were corrected manually by wafting the corner of the single mesh until it was matched with the requirements set for the aspect ratio [4], etc.

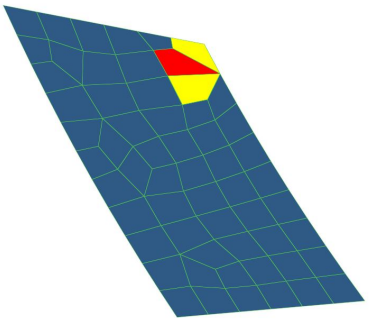

Figure 2.16: The dark blue meshes have good quality. The yellow meshes have good enough quality. The red mesh failed.

- Connectivity between the nodes was checked and the ones that were unconnected were fixed to be connected. This was done on the parts having common edges between the surfaces. For example, the windows are connected to the skin and the meshes have the same edges on the skin, and the windows are supposed to have the same nodes. Otherwise, during the analysis, the windows would not be part of the skin and be going into the space.
- Normal directions of the mesh parts were checked. For a single surface, the normal directions of all parts of the mesh were corrected to be in the same directions.
- Thickness values and material information were assigned per part, see Tables 2.2 and 2.3. Al7050-T7475 was used for all parts. The skin, the stringers, the windows, and the horizontal beams have 1 mm thickness. The frames and the floor beams have 1.27 mm thickness. These values were provided by the

[4] Aspect ratio in HYPERMESH means the ratio of the longest edge of the element to the shortest edge of the element.

engineers in the company, which are the sheet metal manufacturing thickness values. The rails were split into 3 pieces. In Figure 2.15, the green parts on the rails are the sides of the rail which have a 4.5 mm thickness, and the purple part in the middle of the rails is called the center of rails which has a 9.85 mm thickness.

Table 2.2: The mechanical properties of Al7050-T7475 [2].

Mechanical Property	Magnitude	Units
Young's Modulus	70326	N/mm^2
Density	2.81x10E-9	kg/m^3
Poisson's Ratio	0.33	-
Yield Strength	435	N/mm^2
Tensile Strength	505	N/mm^2

Table 2.3: The thickness values of each part.

Part	Thickness (mm)
Skin Stringer Window Horizontal beam	1
Frame Floor beam	1.27
Sides of rails	4.5
Center of rails	9.85

2.2.1 Constraints and Loads

Loads and constraints were created on the models after the meshing and the quality checks were done. The structure needs to be fixed in all 6 degrees of freedom directly or indirectly to constrain the rigid body motion of the structure, otherwise the solver will not converge the solutions ending up with an error. Multi-point constraints (MPC), single-point constraints (SPC), concentrated forces, and distributed pressure forces were applied to the models.

Rigid body elements were created for the windows and fuselage. RBE2 [5] elements were used for both ends of the fuselage since the fuselage model is only a small section of the center fuselage. RBE3 [6] elements were used for the windows to apply

[5]RBE2 (kinematic coupling): RBE2 has an independent node in the middle and the dependent nodes (slave nodes) on both ends of the fuselage. If the motion, like displacement, is observed at the independent nodes, the same motion is observed at all of the dependent nodes. The Slave nodes are rigidly constrained.

[6]RBE3 (distributed coupling): An MPC where the average motion of the independent nodes dominates the motion of the dependent node which does not influence the global stiffness of the whole model.

the load because there are cut-outs in the model to represent windows. For the locations of RBE2 and RBE3, see Figures 2.17 and 2.18.

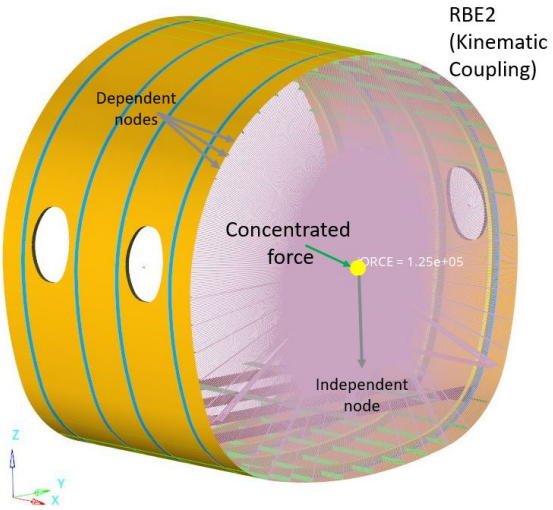

Figure 2.17: RBE2, kinematic coupling, is applied on both end of the fuselage.

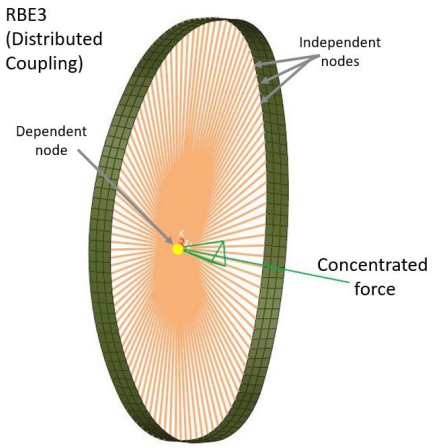

Figure 2.18: RBE3, distributed coupling, is applied on windows.

Single point elements (SPC) were applied to fix the mechanical degrees of freedom for the nodes on the boundaries. These constraints were only applied for the half-scale models CV1(half), CV2(half), DBV1(half), DBV2(half), FBV2(half), and C1DBV1(half). The half-scale models require constrains to satisfy the rigid body motion and also simulate the symmetry. The full-scale model is solved using the inertia relief method.

On the half-scale models, firstly the boundary conditions are applied on the top and on the bottom nodes along the length of the fuselage. Half of the fuselage is modeled and in the case of the other half model existing in reality, the nodes will not move in the y-direction, so the nodes are fixed in the y-direction. These nodes are also constrained in the x-axis and the z-axis to avoid the rotation around them.

On the side which doesn't have the RBE2 element, the displacement is fixed in the x-direction to satisfy the rigid body motion to constrain the model longitudinally. Along that side, the nodes cannot rotate in the y-axis and the z-axis, so these axes are also constrained.

On the side which is having RBE2 element, rotations in the y-axis and the z-axis are fixed. Constraining any displacement on this edge can over-constrain the model and hence there are no translations fixed in this direction. The bottom part of the model is constrained in the z-direction.

The x-direction in the center of the RBE2 element is held intact because the 'x' degree of freedom is associated with the dependent nodes. The other degrees of freedom need to be constrained to solve the problem, hence the other translations and rotations are fixed at the center of the RBE2 element. These type of boundary conditions that are used only to satisfy the problem and does not have a physical significance are called fictitious boundary conditions.

The distributed pressure force applied on the center of the nodes belongs to the skin meshes, see Figure 2.19. Concentrated forces were applied on the RBE2 and RBE3, see Figures 2.17 and 2.18. The forces were applied on each model node, and were calculated by the multiplication of the pressure force and the surface areas of the RBE2 and RBE3 elements of each model. The values are shown in Tables 2.4, 2.5, 2.6 and 2.7. The forces applied on RBE3 elements are the same but they are changing for RBE2 elements since the windows area is assumed to be the same for all models while the fuselage cross-section areas are changing.

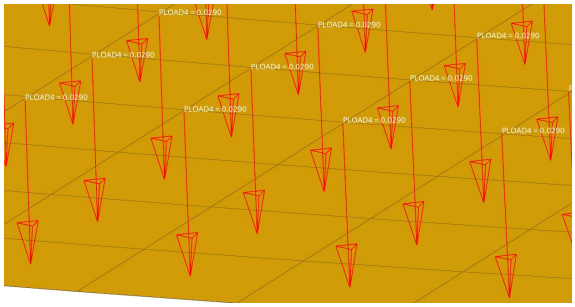

Figure 2.19: The distributed pressure force was applied to the center of each node.

The aircraft is being designed to comply with the certification by EASA under the CS-25 standards. A factor of safety (FOS) is an additional factor applied to the estimated loads to account for the inaccuracies in the methods, materials, approximations used in the design process, etc. The general factor of safety to be accounted for in the whole structure is 1.5 (clause 25.303). Depending on the type of loads and the application region, additional factors need to be accounted for. The factors and procedures needed to be accounted for are described in the CS-25 regulations. According to this clause, the loads used for the design can be categorised as limit loads and design loads, and the regulations are based on the load type.

The limit loads are the maximum loads that an aircraft can experience in its life time. During the design process, the loads acting on the aircraft are estimated using

several methods, after the completion of the design, the aircraft is built and real time data is captured. The maximum loads individually or in combination that can exist on any component that must be accounted for, are called the limit loads. The limit loads might be experienced by the component once or twice during its service. A differential pressure of 4.2 psi is used as a limit load and 8.4 psi is considered as the design load. The distributed pressure load given in psi was converted to N/mm^2 which is 0.029.

Table 2.4: The forces applied on the circular cross-section.

Cross-sections	Versions	RBE2 Force (N)	RBE3 Force (N)	Pressure (N/mm^2)
Circular (CV1) 50 mm frame web height	half	60204	2813	0.029
	full	120408	2813	0.029
Circular (CV2) 75 mm frame web height	half	60204	2813	0.029
	full	120408	2813	0.029

Table 2.5: The forces applied on the double-bubble cross section.

Cross-sections	Versions	RBE2 Force (N)	RBE3 Force (N)	Pressure (N/mm^2)
Double-bubble (DBV1) radius change below the floor	half	58058	2813	0.029
	full	116116	2813	0.029
Double-bubble (DBV2) radius change on the floor	half	58058	2813	0.029
	full	116116	2813	0.029

Table 2.6: The forces applied on the flat bottom cross-section.

Cross-sections	Versions	RBE2 Force (N)	RBE3 Force (N)	Pressure (N/mm^2)
Flat bottom (FBV1) without struts	full	116000	2893.7	0.029
Flat bottom with struts	half	58000	2893.7	0.029
	full	116000	2893.7	0.029

Table 2.7: The forces applied on the comfort double-bubble cross-section.

Cross-sections	Versions	RBE2 Force (N)	RBE3 Force (N)	Pressure (N/mm^2)
Comfort 1 double-bubble (C1DBV1) 50 mm web curve slightly outside	half	59943	2842	0.029
	full	119886	2842	0.029
Comfort 1 double-bubble (C1DBV2) 75 mm web curve slightly outside	full	119886	2842	0.029
Comfort 2 double-bubble (C2DBV1) curve more outside	full	125048	2697	0.029
Comfort 2 double-bubble (C2DBV2) curve more outside	full	125048	2697	0.029
Comfort 2 double-bubble (C2DBV3) curve more outside	full	125048	2697	0.029

2.2.1.1 The Measures to Analyse

The constraints and the loads were applied to the meshed model to analyse the displacements and stresses in FEM. An investigation was carried out on a similar problem at Heart Aerospace, which limits/requires the displacements to not exceed 14 mm and 16 mm for a design load case in the y-axis and z-direction, respectively. Hence, this is used at the maximum allowable limit for displacements in the model.

The stresses studied are the von Mises, major principal (P1 Major), and minor principal (P1 Minor). The von Mises stress gives a weighted average of the stress at a certain location. The major principal stress provides an idea of the tensile stresses in the model and to follow a conservative approach, the highest of the two stresses is chosen for the design. The minor principal stress provides the minimum normal stress which is the compression stress. It was also checked to see the results of the different cross-sections and to be on the safe side.

2.3 Drag Estimation

The steps for the drag estimation are given below. The total drag coefficient C_D is shown in Equation 2.1, chapter 15 of General Aviation Aircraft Design [19]. C_{DO} is the pressure drag coefficient, C_{Df} is the skin friction coefficient, C_{Di} is the induced drag coefficient, C_{Dw} is t he wave drag and C_{Dmisc} is the miscellaneous drag which represents any additional drag. The induced drag was not accounted for in this study since it is drag due to the lift provided by the wing. Only the friction drag

and the pressure drag were calculated in this study that has the predominant effect on the fuselage.

$$C_D = C_{DO} + C_{Df} + C_{Di} + C_{Dw} + C_{Dmisc} \tag{2.1}$$

The friction drag is the drag due to the air sticking to the skin of the aircraft. The shear force of the air flowing over the surface causes this drag. It is calculated by Equation 2.2. D_f is the drag force, ρ is the density of the air at the given altitude, V_∞ is the free stream velocity of the aircraft, C_f is the coefficient of friction, S_{wet} is the wetted area of the body and S_{ref} is the reference area. The coefficient of friction for a turbulent flow is given by the equation 2.3 where R_e is Reynold's number and M is the Mach number.

$$C_{Df} = \frac{2D_f}{\rho V_\infty^2 S_{ref}} = C_f \frac{S_{wet}}{S_{ref}} \tag{2.2}$$

$$C_{fturb} = \frac{0.455}{(\log 10 R_e)^{2.58}(1 + 0.144M^2)^{0.65}} \tag{2.3}$$

The pressure drag is the drag induced due to the shape of the object. The air pressure on the frontal area causes a backward force inducing drag. It is given by the equation 2.4 where d_b is the base diameter at the rear of the fuselage and d is the average diameter of the fuselage.

$$C_D = \frac{0.029 \frac{(d_b}{d})^3}{\sqrt{(C_{Df})}} \tag{2.4}$$

The total coefficient of drag is the sum of the friction drag and the pressure drag.

3

Results

In this section, the resulting displacements and stresses from the FE analysis are included. The comparisons of the weight of assemblies and the drag coefficients are also comprised.

The displacement near the windows is very high and not realistic for all the models, since the models do not include adequate stiffening near the windows. Hence, the displacement in the y-direction is chosen from the node placed between the two frames which are not influenced by the deflection in the windows as shown in Figure 3.1. The z-displacement was taken at the top and the bottom of the frame which has a higher tendency to deflect in the vertical direction.

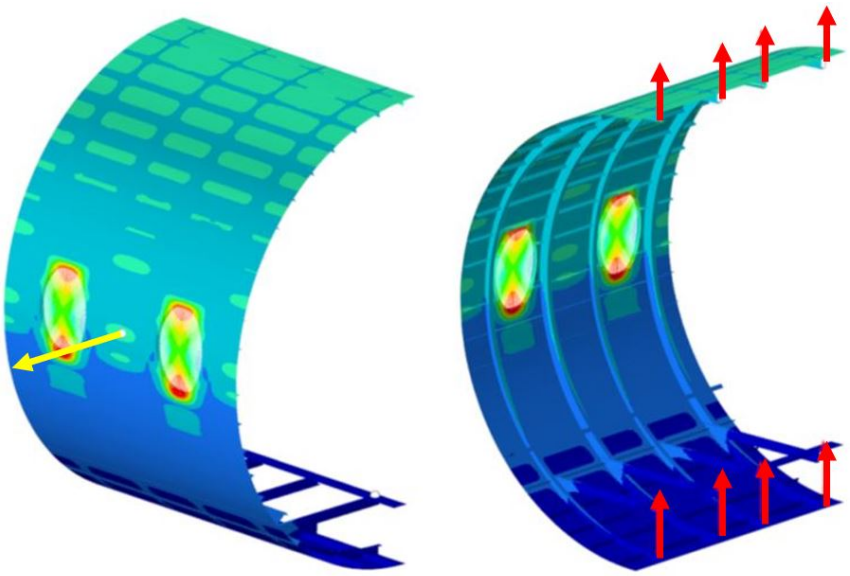

Figure 3.1: Locations at which Y and Z displacements are noted.

The von Mises stress, major principal stress, and minor principal stress were studied. The stress magnitudes viewed are the average stress which is a result of the average stress from all the nodes in the element. The models do not include the parts as in the real structure and only consider the mass distribution at certain locations. This causes the stresses to be concentrated at the joints and sharp corners. So, the stress in such elements is neglected.

3.1 Circular Cross-section

Two versions of the circular cross-section were analyzed using full-scale models and half-scale models. The tendency of the displacements and the stresses are similar for the two versions of the circular cross-section model. The stresses are highest near the window frames, see Figure 3.2. The pressure load causes the top and the bottom of the frame to deflect vertically outwards and the sides of the fuselage to compress inwards. The displacements and the stresses are shown in Tables 3.1 and 3.2.

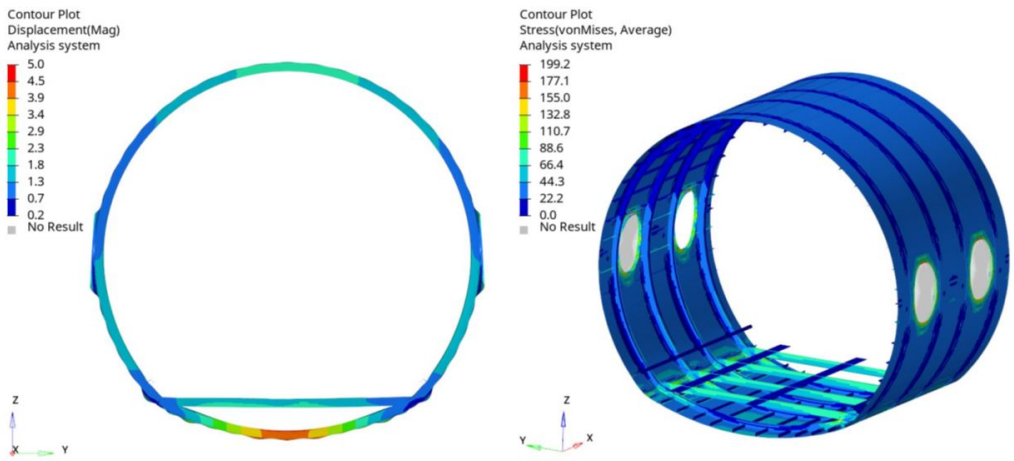

Figure 3.2: Displacement shape and stress in the circular model (50 mm web height), 1DP

3.1.1 Displacement

The maximum displacement is 2.195 mm for the 1DP load case which is seen in version CV1. The displacements in the y-axis are higher for the full-scale models and the z-axis is higher for the half-scale models. The minimum y-displacement is 50% smaller than the maximum value. The minimum z-displacement is 24% smaller than the maximum value. The displacement values for load case 2DP are twice the displacements for load case 1DP with a small variation in the hundredth decimal.

3.1.2 Stress

In the 1DP load condition, the lowest value for the von Mises stress is 47.7 MPa for the CV1 half-scale model, for the P1 Major stress is 42.6 MPa for CV2 half-scale model, and for the P3 Minor stress is 24.7 MPa for CV2 half-scale again. The highest value for the von Mises stress is 81.9 MPa, and the P1 Major stress is 63.9 MPa both of them were obtained from CV2 full-scale model. The highest value for the P3 Minor stress is 28.8 MPa for CV1 half-scale model.

CV2, which has a 75 mm frame web height, has higher stresses in the structure compared to CV1. Increasing the web height provides a very slight benefit in terms

of displacement, however, the stress experienced is higher.

Table 3.1: The maximum displacement values of each circular cross-section model for the y-axis and the z-axis under the load conditions 1DP and 2DP.

		1DP		2DP	
Cross-sections	Versions	y axis (mm)	z axis (mm)	y axis (mm)	z axis (mm)
Circular (CV1) 50 mm frame web height	half	1.113	1.105	2.226	2.209
	full	2.195	0.1514	4.389	0.3029
Circular (CV2) 75 mm frame web height	half	0.6769	0.9075	1.354	1.815
	full	1.127	0.6424	2.254	1.285

Table 3.2: The average values of von Mises stress, P1 Major stress, and P3 Minor stress in MPa of each circular cross-section model under the load conditions 1DP and 2DP.

		1DP (MPa)			2DP (MPa)		
Cross-sections	Versions	von Mises	P1 Major	P3 Minor	von Mises	P1 Major	P3 Minor
Circular (CV1) 50 mm frame web height	half	47.7	45.9	28.8	95.4	91.9	57.5
	full	50.75	44.15	26.6	101.5	88.3	53.2
Circular (CV2) 75 mm frame web height	half	42.8	42.6	24.7	91.9	85.2	49.4
	full	44.3	41.9	25	88.5	83.1	50.06

3.2 Double-Bubble Cross-section

Two versions of the double-bubble cross-section were analyzed using full-scale models and half-scale models. The tendency of the displacements and the stresses are similar for the two versions of the double-bubble cross-section model. The stresses are highest near the window frames. The stresses in both versions are higher at the point of transition, see Figure 3.3. The displacements and stresses are shown in Tables 3.3 and 3.4.

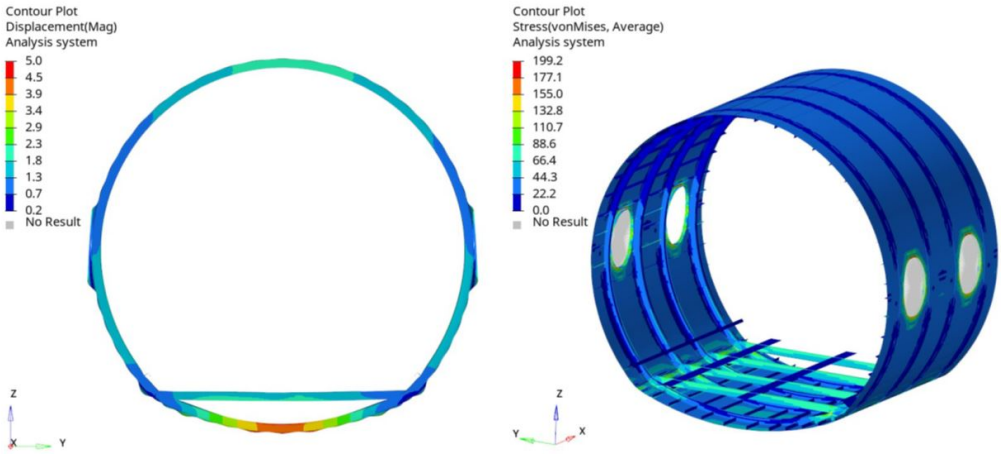

Figure 3.3: Displacement shape and stress in the double-bubble model, 1DP

3.2.1 Displacement

The maximum displacement is 7.23 mm for the 1DP load case which is seen in the full-scale model of version DBV2. The displacements in the z-direction are significantly higher than the ones in the y-direction. The same is observed for both the half-scale models and the full-scale models. The displacement values for the y-direction of DBV2 are lower than DBV1. The displacement values for the z-direction of DBV2 are higher than DBV1. But, the magnitude of variation in the displacement is small.

3.2.2 Stress

In the 1DP load condition, the lowest value for the von Mises stress is 141.65 MPa for DBV2 half-scale model, for the P1 Major stress is 117 MPa for the DBV1 half-scale model and for the P3 Minor stress is 28.75 MPa for DBV1 full-scale again. The highest value for the von Mises stress is 249 MPa, and the P1 Major stress is 240 MPa both of them were obtained from the DBV1 full-scale model. The highest value for the P3 Minor stress is 49.7 MPa for DBV2 full-scale model. The magnitude of variation in the stress between the half-scale model and the full-scale model is significantly high compared to DBV1.

Table 3.3: The maximum displacement values of each double-bubble cross-section model for y and z axis under the load conditions 1DP and 2DP.

		1DP		2DP	
Cross-sections	Versions	y axis (mm)	z axis (mm)	y axis (mm)	z axis (mm)
Double-bubble (DBV1) radius change below the floor	half	0.85	5.48	1.71	10.97
	full	2.86	6.62	5.72	13.24
Double-bubble (DBV2) radius change on the floor	half	0.68	6.8	1.36	13.62
	full	2.158	7.23	4.317	14.47

Table 3.4: The The average values of von Mises stress, P1 Major stress, and P3 Minor stress of each double-bubble cross-section model under the load conditions 1DP and 2DP.

		1DP (MPa)			2DP (MPa)		
Cross-sections	Versions	von Mises	P1 Major	P3 Minor	von Mises	P1 Major	P3 Minor
Double-bubble (DBV1) radius change below the floor	half	164	117	33.39	327	233	66.78
	full	249	240	28.75	499	481	57.5
Double-bubble (DBV2) radius change on the floor	half	141.65	147.35	42.1	283.3	294.7	84.2
	full	148.7	154.6	49.7	297.4	309.1	99.45

3.3 Flat Bottom Cross-section

Two versions of the flat bottom cross-section were analyzed using half-scale models for both and full-scale models only for the second version. The displacement for the flat bottom cross-sections (with and without struts) is shown in Figure 3.4. The maximum displacement values are seen on the skin for 2 versions of this cross-section. The maximum stress values are observed at the location of the change in the curvature from circle to flat profile, see Figure 3.5. The displacements and stresses are shown in Tables 3.5 and 3.6.

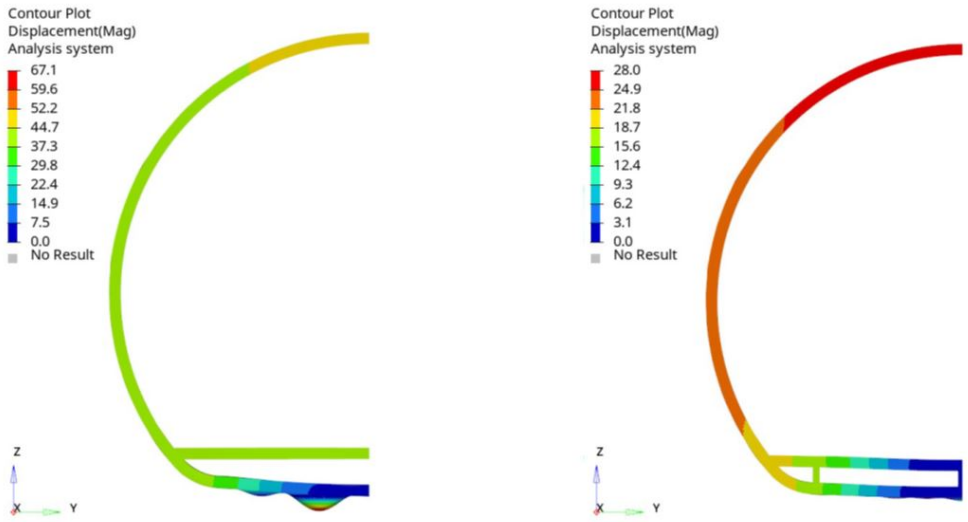

Figure 3.4: Displacement shape in the flat bottom model (without struts on left and with struts on right), 1DP

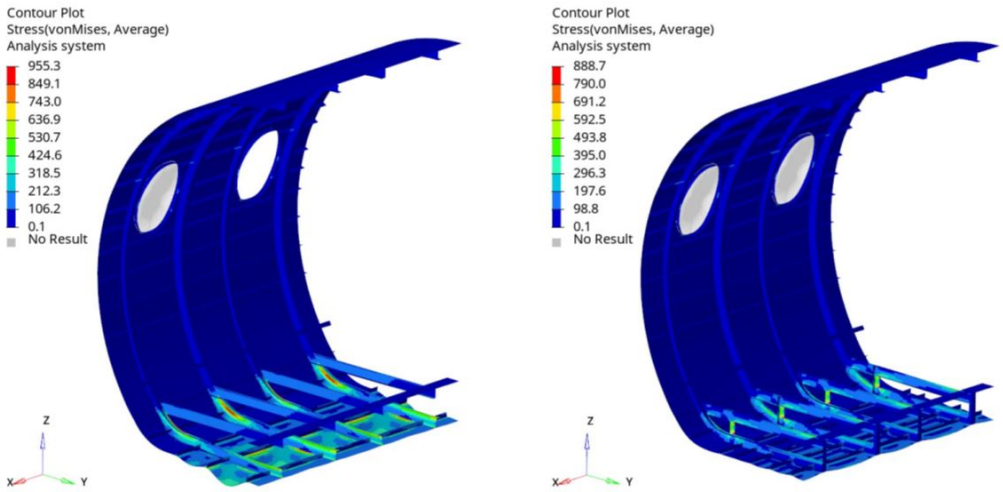

Figure 3.5: Stress in the flat bottom model (without struts on left and with struts on right), 1DP

3.3.1 Displacement

The maximum displacement is 45.7 mm for the 1DP load case which is seen in the half-scale model of the first version, FBV1. The displacement in the z-axis is very high compared to the y-axis. Adding the struts reduces the displacement to only 3 mm in the z-direction for the load case 1DP. Overall, the displacements are higher at the bottom part of this cross-section model where the profile is straight.

3.3.2 Stress

The version without struts, FBV1 is having the highest von Mises stress value for the 1DP load condition. When the struts are added, this stress value is decreasing by 37%.

Table 3.5: The maximum displacement values of each flat bottom cross-section model for y and z axis under the load conditions 1DP and 2DP.

		1DP		2DP	
Cross-sections	Versions	y axis (mm)	z axis (mm)	y axis (mm)	z axis (mm)
Flat bottom (FBV1) without struts	half	5.89	45.7	11.79	91.5
Flat bottom (FBV2) with struts	half	6.049	28	12.1	56.01
	full	5.85	42.54	11.72	84.11

Table 3.6: The average values of von Mises stress, P1 Major stress, and P3 Minor stress in MPa of each flat bottom cross-section model under the load conditions 1DP and 2DP.

		1DP (MPa)			2DP (MPa)		
Cross-sections	Versions	von Mises	P1 Major	P3 Minor	von Mises	P1 Major	P3 Minor
Flat bottom (FBV1) without struts	half	949.8	956	74.43	1898	1912	148.9
Flat bottom (FBV2) with struts	half	609	583	82	1218	1166	163
	full	614	589	83.4	1228	1177	167

3.4 Comfort Double-Bubble Cross-section

Five versions of the comfort double-bubble cross-section were analyzed using full-scale models for all and half-scale models for the first version, C1DBV1.

The displacement and stress for the first version C1DBV1 can be seen in Figure 3.6, for the 1DP load case. The stress is higher at the location of the change in the cross-section on the side and belly. The displacements and stresses are shown in Tables 3.7 and 3.8.

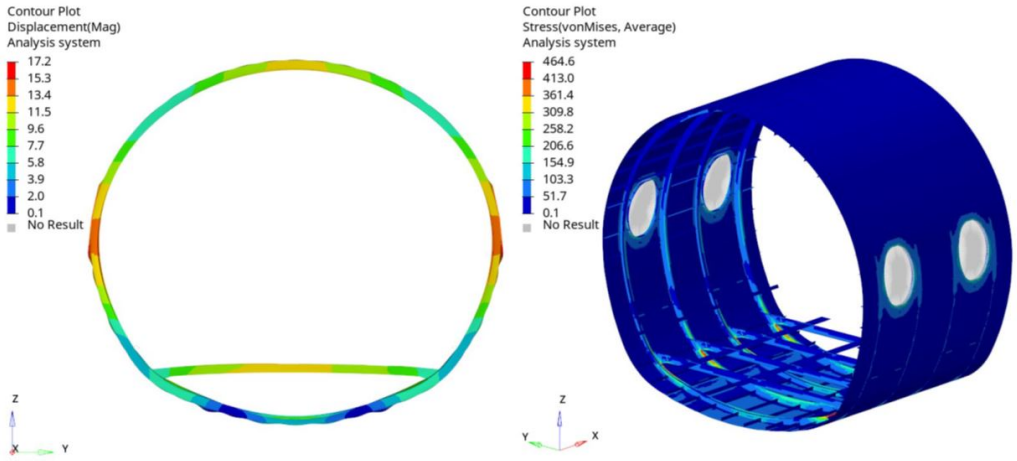

Figure 3.6: Displacement and stress for Comfort 1, 50mm web height for load 1DP

3.4.1 Displacement

The first version of this cross-section, C1DBV1, has the maximum deflection values on both the y-axis and z-axis for load case 1DP. An increase in the frame web height from 50 mm to 75 mm is decreasing the displacement values for comfort 1 double-bubble cross-sections.

3.4.2 Stress

The first version of this cross-section, C1DBV1, is also having the maximum stress values for the von Mises stress, P1 Major stress, and P3 Minor stress. The increase in the frame web height from 50 mm to 75 mm is again decreasing the stress values for comfort 1 double-bubble cross-sections.

The comfort 2 double-bubble cross-section has similar stresses in all the versions, C2DBV1, C2DBV2, and C2DBV3, as in the case of displacement. The von Mises and P1 Major stress values are quite close except for version C2DBV3.

Table 3.7: The maximum displacement values of each comfort double-bubble cross-section model for y and z axis under the load conditions 1DP and 2DP.

		1DP		2DP	
Cross-sections	Versions	y axis (mm)	z axis (mm)	y axis (mm)	z axis (mm)
Comfort 1 double-bubble (C1DBV1) 50 mm web height curve slightly outside	half	11.34	7.31	22.68	14.62
	full	13.65	13.41	27.3	26.83
Comfort 1 double-bubble (C1DBV2) 75 mm web height curve slightly outside	full	5.16	2.34	10.34	4.68
Comfort 2 double-bubble (C2DBV1) 50 mm web height curve more outside	full	9.12	2.36	18.95	4.72
Comfort 2 double-bubble (C2DBV2) 75 mm web height curve more outside	full	9.47	0.59	18.43	1.18
Comfort 2 double-bubble (C2DBV3) variable frame web height curve more outside	full	9.21	0.65	18.4	1.31

Table 3.8: The average values of von Mises stress, P1 Major stress, and P3 Minor stress in MPa of each comfort double-bubble cross-section model under the load conditions 1DP and 2DP.

		1DP (MPa)			2DP (MPa)		
Cross-sections	Versions	von Mises	P1 Major	P3 Minor	von Mises	P1 Major	P3 Minor
Comfort 1 double-bubble (C1DBV1) 50 mm frame web height curve slightly outside	half	357	345	46.05	714	689	92.1
	full	441	426	55.71	883	851	111.44
Comfort 1 double-bubble (C1DBV2) 75 mm frame web height curve slightly outside	full	258	250	36.86	515	500	73.73
Comfort 2 double-bubble (C2DBV1) 50 mm frame web height curve more outside	full	295.6	297	45.68	953	869	91.36
Comfort 2 double-bubble (C2DBV2) 75 mm frame web height curve more outside	full	287	270	36.92	574	540	73.85
Comfort 2 double-bubble (C2DBV3) variable frame web height curve more outside	full	286	232	33.4	572	463	66.8

3.5 Finite Element Analysis Result Comparison

The displacements for the load 1DP and 2DP on the y-axis and the z-axis can be seen in Figures 3.7 and 3.8, respectively. In general, the magnitude of displacement on the z-axis is higher than the displacement on the y-axis for the same point. The z and y axes are always the same for all the components. The acceptable value for the displacement is 14 mm on the y-axis and 16 mm on the z-axis. The flat bottom cross-section and the comfort 1 cross-sections do not qualify for this category. The circular cross-section has the minimum displacements when compared to the other cross-sections. The only two cross-sections meeting the displacement limits in both directions are the circular cross-sections and double-bubble cross-sections.

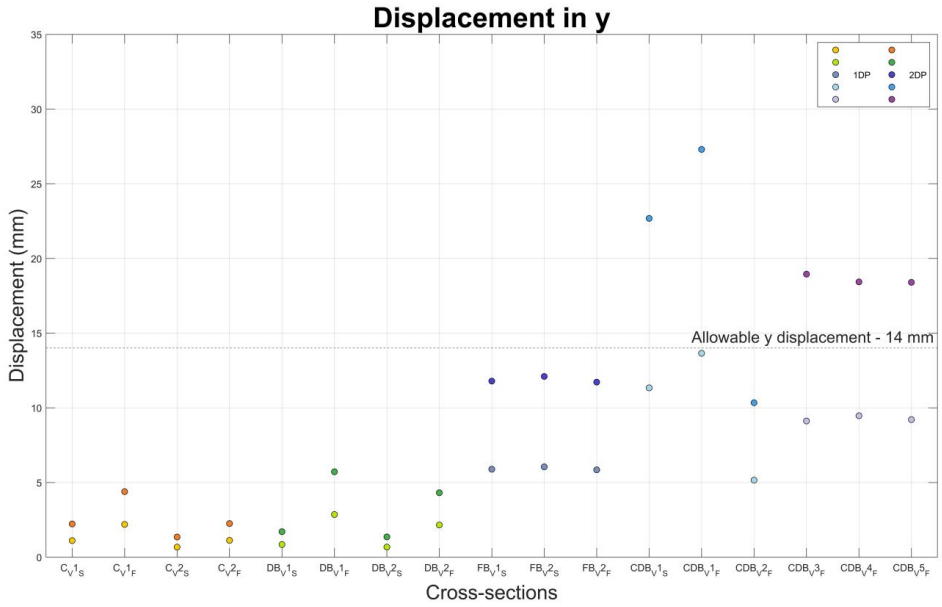

Figure 3.7: Comparison of displacement in y-axis for load 1DP and 2DP

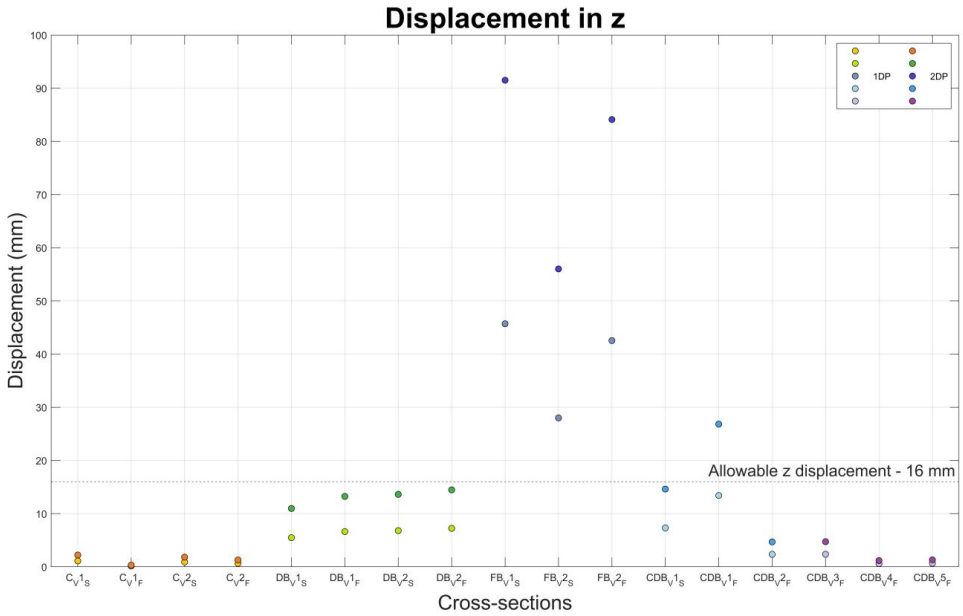

Figure 3.8: Comparison of displacement in z-axis for load 1DP and 2DP

The von Mises stress, P1 Major stress, and P3 Minor stress for the load 1DP and 2DP can be seen in Figures 3.9, 3.10 and 3.11, respectively. The circular cross-section has the minimum values for the stresses compared to all the other cross-sections. The flat bottom cross-section has the maximum stresses especially in the model without struts. P3 Minor stress is showing the stress for the compression in the models which is having the minimum value in the circular cross-section. The flat bottom cross-section has the maximum stress values for compression.

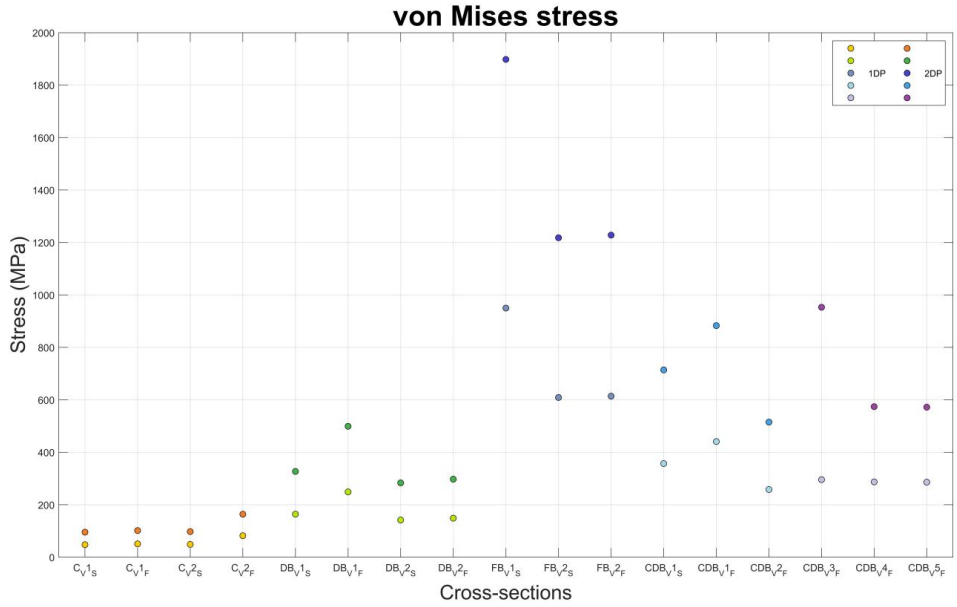

Figure 3.9: Comparison of von Mises stress for load 1DP and 2DP

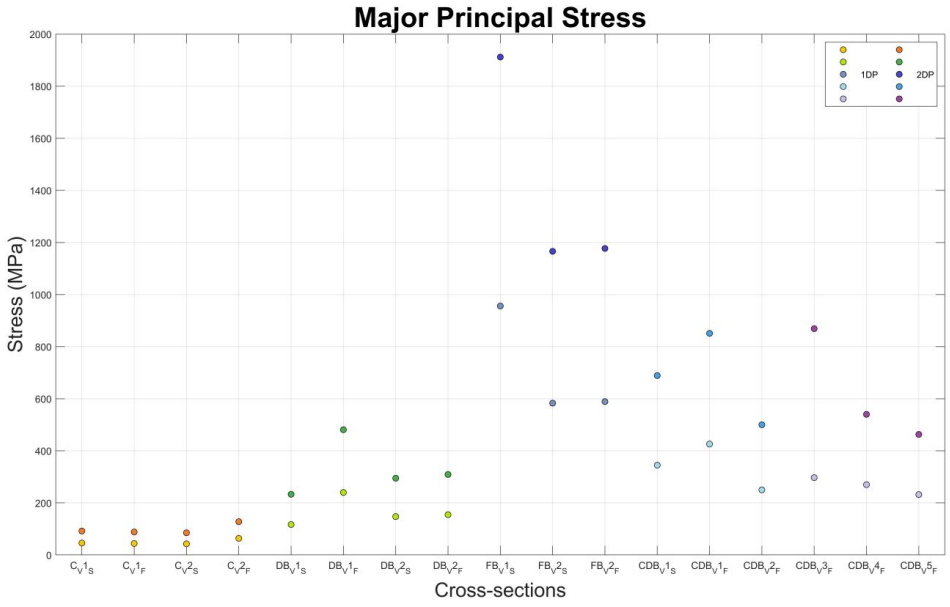

Figure 3.10: Comparison of major principal stress for load 1DP and 2DP

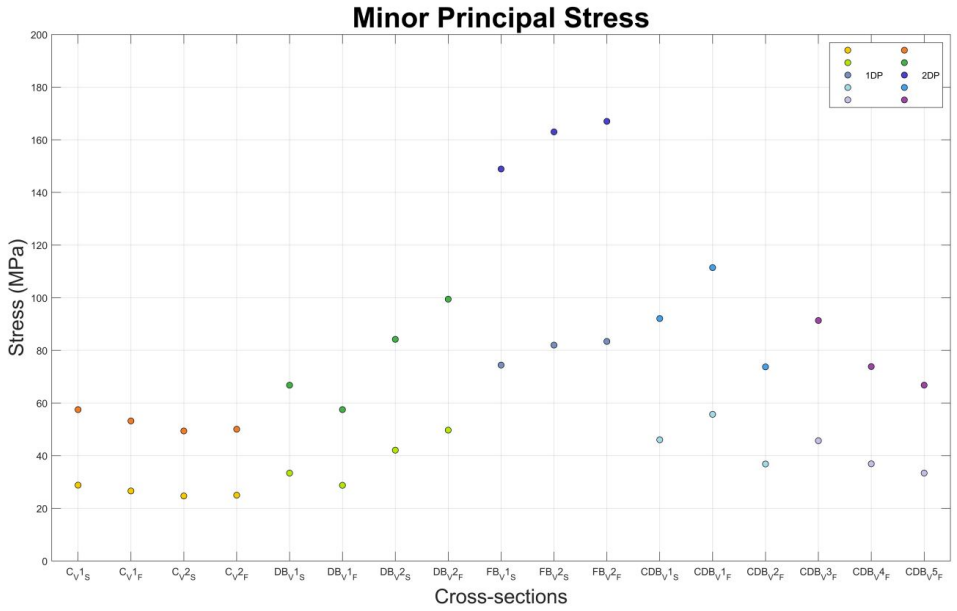

Figure 3.11: Comparison of minor principal stress for load 1DP and 2DP

3.6 Drag

The skin friction drag coefficients and the pressure drag coefficients were calculated to give the total drag coefficient results. The total length of the aircraft, 21.473 m, and the center fuselage section, 13.047 m, were assumed the same for all the models. In Table 3.9, the cross-section comfort 2 double-bubble has the maximum total drag coefficient value of $7.70 \cdot 10^{-3}$ and the cross-section flat bottom has the minimum total drag coefficient value of $7.59 \cdot 10^{-3}$. There is no significant difference between the models.

Table 3.9: The drag coefficients of each model.

		Drag		
Cross section	Versions	Skin Friction	Pressure	Total
Circular	CV1, CV2	$3.96 \cdot 10^{-3}$	$3.69 \cdot 10^{-3}$	$7.64 \cdot 10^{-3}$
Double-Bubble	DBV1	$3.92 \cdot 10^{-3}$	$3.70 \cdot 10^{-3}$	$7.63 \cdot 10^{-3}$
Double-Bubble	DBV2	$3.90 \cdot 10^{-3}$	$3.72 \cdot 10^{-3}$	$7.61 \cdot 10^{-3}$
Flat Bottom	FBV1, FBV2	$3.86 \cdot 10^{-3}$	$3.73 \cdot 10^{-3}$	$7.59 \cdot 10^{-3}$
Comfort 1 Double-Bubble	C1DBV1, C1DBV2	$3.97 \cdot 10^{-3}$	$3.68 \cdot 10^{-3}$	$7.65 \cdot 10^{-3}$
Comfort 2 Double-Bubble	C2DBV1, C2DVB2 C2DBV3	$4.05 \cdot 10^{-3}$	$3.64 \cdot 10^{-3}$	$7.70 \cdot 10^{-3}$

3.7 Weight

The total weight of each cross-section full-scale model is shown in Table 3.10. The models FBV1 and DBV1 have the minimum and almost the same value which is

50.8 kg. The model C2DBV3 has a maximum weight of 55.7 kg. Weight values were calculated for a fuselage length of 1520 mm which are only for comparison and not reflecting the proper and real weight of an aircraft.

Table 3.10: The total weights of each model.

Cross-section	Version	Weight (kg)
Circular	CV1 50 mm frame web height	51.9
	CV2 75 mm frame web height	53.3
Double-bubble	DBV1 radius change below the floor	50.8
	DBV2 radius change on the floor	51.0
Flat bottom	FBV1 without struts	50.8
	FBV2 with struts	51.0
Comfort 1 double-bubble curve slightly outside	C1DBV1 50 mm frame web height	51.7
	C1DBV2 75 mm frame web height	54.1
Comfort 2 double-bubble curve more outside	C2DBV1 50 mm frame web height	52.6
	C2DBV2 75 mm frame web height	55.1
	C2DBV3 variable frame web height	55.7

4

Discussion

The project revolves around defining the optimum cross-section for the fuselage with internal pressure. The fuselage is a pressure vessel and a circular cross-section is optimum for such scenarios. Using this as the foundation, the profile was altered by means of a trial and error approach to arrive at different cross-sections. The cross-sections have been manually defined and a finite element analysis was carried out on each model. The data in this project is only used to establish the differences in several design methodologies for the cross-section of the fuselage in the chosen class of aircraft. A limited number of cross-section profiles considered for the analysis is acceptable to establish the differences between several cross-section profiles.

An aircraft is operated in adverse weather conditions, different altitudes, turbulent gusts of wind, etc. The loading on the fuselage is quite complex, and several load cases need to be considered for the design. But, the predominant design driving criteria for the cross-section of the fuselage is the differential pressure which is considered in the study. As the study only focuses on the outer profile of the fuselage, and does not include the detailed design of the fuselage, the consideration of just the differential pressure is justifiable.

The project has relevance in the conceptual design phase of the aircraft, hence the finite element analysis does not include the real stiffness 100% as in the real structure. The reason for it is the final manufacturable design will include a lot of details which is not accounted for in the course of this work. The major structural components are considered for the analysis and the comparison between different cross-sections is ensured by maintaining the same properties and thickness for all the structural elements. So, the results obtained from the FEA can be used for comparing the different design methodologies under investigation.

Comparing the solutions, the circular cross-section has an upper hand over the other cross-section profiles in terms of displacements and stresses experienced in the model. The uniform circular profile ensures a uniform pressure distribution over the entire circumference of the fuselage, leading to lower displacement values and hence low stresses. On the other hand, the increase in the web height from 50 mm to 75 mm increases the stiffness and reduces the maximum displacement in the model. Also, the increase in the web height causes higher stresses in the frames. Even though this increase is below the allowable limit, which is not a good solution. To summarize, the circular cross-section is a suitable profile in terms of stiffness. In terms of an efficient design, the circular cross-section is not an ideal option. But since the frontal area is higher than necessary and the area under the floor can be reduced resulting in lower weight and drag.

The double-bubble cross-section seems to be promising in different aspects. Firstly, the displacements are close to 2 mm and the stresses in the second version are approximately 150 MPa. The values are low because the double-bubble cross-section still maintains a circular profile except at the transition points. Secondly, the weight of the model is less due to the low cross-section area. The placement of the floor plays a key role in designing a double-bubble cross-section. Placing the floor beam at the transition of the radius relieves the stresses significantly. The first version of the double-bubble cross-section has almost 75% higher magnitude in terms of stresses compared to the second version while maintaining the same dimension, outer profile, and thickness.

The flat bottom cross-section has the highest displacements which are very large compared to other cross-sections. The displacement for the design load case is nearly 12 mm, which is unacceptable. This results in the stress of the magnitude of 1800 MPa which is unrealistically high and indicates a significant yielding. The considered dimensions are not modified to take the applied loads, however, when compared with the other cross-sections, the flat bottom cross-section has a major downside. It can be seen in this example that the flat profile is poor in handling pressure loads. Since stiffness plays an important role in the design, this model can be neglected for further comparison.

The first version of the comfort cross-section, with the 50 mm web height has higher displacements as in the case of a flat profile. But, increasing the web height improves the stiffness of the model. The displacement and stress levels are below the allowable limit, but still higher than the circular or double-bubble cross-section. This model majorly provides comfort to the passenger in flight. The increase in the width of the fuselage for the second version has higher magnitudes of displacement and stress. This is due to the flat profile in the cross-section and as viewed in the flat bottom cross-section, a flatter profile decreases the stiffness.

To summarize, it can be seen that the double-bubble has slightly higher displacements and stress compared to the circular cross-section, but is under the allowable limit. The double-bubble has an advantage in terms of frontal area and weight. As a whole, the slight compromise in the stiffness can provide better drag performance, so the double-bubble structure is considered better. Comparing this with the comfort cross-section, the comfort cross-section, as the name suggests, provides better comfort to the passenger. But, the class of aircraft being designed is operated for short distances, only a couple hours of flight. A small compromise in comfort can result in better efficiency and fewer carbon dioxide emissions. Thus, it can be concluded that the double-bubble cross-section is a good design that can be used in the design of the fuselage.

5
Conclusion

The cross-section of the fuselage in an aircraft impacts the passenger comfort, drag, and weight. The last two factors have an impact on the performance of the aircraft. So it is important to choose a cross-section for the best possible performance without compromising too much on the passenger comfort. A trial and error approach is followed to choose possible cross-sections for short-haul commercial air travel with 2+1 seats abreast. A finite element analysis has been carried out to study the stiffness of the structure, the stress, weight, and drag for internal pressure. These parameters are compared to deduce an optimum design for the cross-section of the fuselage.

Four cross-sections have been studied: circular, double-bubble, flat bottom, and comfort (manually defined for best comfort) cross-section. The circular cross-section has the least displacements and stresses in the model, making it a very stiff and durable design. However, the area below the floor is not completely utilized and the shape can be optimized for weight saving. The double-bubble structure has slightly higher displacement and stresses than the circular cross-section. The flat-bottom cross-section shows a significantly higher deformation, so it is not a good solution. The comfort cross-sections have a small deformation and are comparable with the double-bubble cross-section, but the stresses are higher than the double-bubble structure because of multiple changes in cross-sections. The stiffening required for this model in comparison with the double-bubble structure is higher. Also, with all simplified analyses and all uncertainties, there is no significant difference can be predicted for the drag results of the different models.

To summarize, the double-bubble structure is better than the circular in terms of weight with a small compromise in stiffness. The double-bubble structure is also better than the comfort cross-sections in terms of stress experienced with a small compromise on passenger comfort. It is also important to ensure that the floor is placed at the location of the change in the profile for a double-bubble structure. So, it can be concluded that a double-bubble profile is best for the design of the fuselage for a short-haul commercial aircraft with a 2+1 seat abreast.

6
Future Work

This project is carried out in the initial phase of the aircraft conceptual design. The data available in this stage of the design is quite limited. However, with more time invested in the work further, there is a scope to study more in detail as discussed in this section.

The project considers a standard fuselage section with equal frame spacing to calculate the displacement. The frame spacing is dominated by the stringer buckling criteria. The skin stringer panel between the two frames is critical due to buckling. The relation between the buckling might be observed in the stringer versus the length is an interesting problem to be studied.

The analysis is carried out on the frames with a C-section. The section of the frame has a big impact on the design of the fuselage and the impact of using different sections (such as L-section, and H-section) can also be studied. The thickness of the frame is maintained the same for all the sections will be tried, then the sizing of the structure for stresses can be performed for the comparison.

The position of the floor beam and the cross-section used for the floor beam is another topic for study. The fuselage modelled is an ideal scenario, however, the structure, in reality, is more complex. The effect of the cross-section at these locations needs to be performed as it determines the actual cross-section profile to be used.

The load considered in the study is a simplified load case, but the load, in reality, is a significantly complex load and the effect of the combination of such load cases on the structure needs to be studied. The structures used in the model have a coincident structure, however, in practical application, the contact between the structures is through a fastener and the contact analysis is performed. However, this will require a detailed design of the structure.

The displacement and the stress results difference for the full-scale model and the half-scale model are significant for some models. That means something should be investigated to explain these differences.

Bibliography

[1] Heart Aerospace. Electrifying Regional air travel; 2022. Available from: https://heartaerospace.com/.

[2] MatWeb. Material Property Data-Aluminum 7475-T61; 2015. Available from: https://www.matweb.com/search/DataSheet.aspx?MatGUID=9301e602923c4bca973c5856a82249ca.

[3] EASA. European Union Aviation Safety Agency (EASA); 2022. Available from: https://european-union.europa.eu/institutions-law-budget/institutions-and-bodies/institutions-and-bodies-profiles/easa_en.

[4] Embraer. Emraer 145 Cabin Interior; 2022. Available from: file:///C:/Users/sena.otlu/Downloads/ERJ%20145%20Info%20(2).pdf.

[5] EASA. Type Certificate Data Sheet for Virus SW 121. Type Certificate Data Sheet. 10 June 2020;EASA.A.573(05):1-12.

[6] Gulfstream. The Gulfstream G650 Family; 2022. Available from: https://www.gulfstream.com/en/aircraft/gulfstream-g650er/.

[7] Bombardier. Bombardier Global Express; 2022. Available from: https://www.fly-efi.com/our-fleet/largecabin/Global-Express.php.

[8] Gulfstream. Gulfstream Aerospace Gulfstream G550; 2022. Available from: https://www.globalair.com/aircraft-for-sale/specifications?specid=1050.

[9] Antonov. AN-148-201 Regional Passanger Aircraft; 2022. Available from: https://antonov.com/en/aircraft/an-148-201.

[10] Embraer. Emraer Lineage 1000; 2022. Available from: https://globaljet.aero/en/embraer-lineage-1000.

[11] Bryan R Swopes. Tissandier Electric Airship; 2018. Available from: https://www.thisdayinaviation.com/tag/tissandier-electric-airship/.

[12] Alice. Scylax Green Aviation; 2020. Available from: https://www.scylax.eu/.

[13] Alice. Alice; 2022. Available from: https://www.eviation.com/.

[14] Auro Aero. 19 Seat Electrical Regional Aircraft; 2022. Available from: https://aura-aero.com/en/era/#characteristics.

[15] 3DEXPERIENCEedu. CATIA V5 STUDENT EDITION; 2022. Available from: https://edu.3ds.com/en/software/catia-v5-student-edition.

[16] Altair. Documentation Altair product manuals, release notes, guides, tutorials, model files; 2022. Available from: https://support.altair.com/csm?id=altair_product_documentation&spa=1&filter=product%3D5c069018db0348102af07608f496192f%5EORproduct%3Dd8069018db0348102af07608f496192b&p=1&d=asc.

[17] Altair. Altair Hyperworks User's Guide; 2022. Available from: https://2021.help.altair.com/2021/hwdesktop/altair_help/topics/tools/hvvh_user_guide_r.htm.

[18] NX Nastran. NX Nastran User's Guide; 2022. Available from: https://docs.plm.automation.siemens.com/data_services/resources/nxnastran/10/help/en_US/tdocExt/pdf/User.pdf.

[19] Gudmundsson S. General Aviation Aircraft Design: Applied Methods and Procedures; 2021.

DEPARTMENT OF SOME SUBJECT OR TECHNOLOGY
CHALMERS UNIVERSITY OF TECHNOLOGY
Gothenburg, Sweden
www.chalmers.se

CHALMERS
UNIVERSITY OF TECHNOLOGY